

Article

Polyurethane/Silane-Functionalized ZrO₂ Nanocomposite Powder Coatings: Thermal Degradation Kinetics

Farimah Tikhani ¹, Behzad Shirkavand Hadavand ^{2,*}, Hamed Fakharzadeh Bafghi ², Maryam Jouyandeh ³, Henri Vahabi ³ , Krzysztof Formela ⁴ , Hossein Hosseini ⁵, Seyed Mohammad Reza Paran ⁶, Amin Esmaeili ⁷ , Ahmad Mohaddespour ⁸ and Mohammad Reza Saeb ^{2,*} 

¹ School of Chemical Engineering, College of Engineering, University of Tehran, Tehran 11155-4563, Iran; farimah.tikhani@gmail.com

² Department of Resin and Additives, Institute for Color Science and Technology, Tehran 16765-654, Iran; hamed.fakharzadeh@gmail.com

³ Université de Lorraine, CentraleSupélec, LMOPS, F-57000 Metz, France; maryam.jouyande@gmail.com (M.J.); henri.vahabi@univ-lorraine.fr (H.V.)

⁴ Department of Polymer Technology, Faculty of Chemistry, Gdańsk University of Technology, Gabriela Narutowicza 11/12, 80-233 Gdańsk, Poland; krzysztof.formela@pg.edu.pl

⁵ Department of Chemical Engineering, Abadan Branch, Islamic Azad University; P.O. Box 467, Ardabil 6317836531, Iran; pedram465@yahoo.com

⁶ Advanced Materials Group, Iranian Color Society (ICS), Tehran 1591637144, Iran; smrparan@gmail.com

⁷ Department of Chemical Engineering, School of Engineering Technology and Industrial Trades, College of the North Atlantic–Qatar, 24449 Arab League St, Doha 24449, Qatar; amin.esmaeili@cna-qatar.edu.qa

⁸ Department of Chemical Engineering, College of Engineering and Technology, American University of Middle East, P.O. Box 220, Dasman, 15453 Egaila, Kuwait; ahmad.mohaddespour@mail.mcgill.ca

* Correspondence: shirkavand@icrc.ac.ir (B.S.H.); saeb-mr@icrc.ac.ir or mrsaeb2008@gmail.com (M.R.S.); Tel.: +98-21-2295-6209-x146 (M.R.S.); +98-21-2295-6209 (B.S.H.); Fax: +98-21-2294-7537 (M.R.S.); +98-21-2294-7537 (B.S.H.)

Received: 19 March 2020; Accepted: 14 April 2020; Published: 21 April 2020



Abstract: A polyurethane (PU)-based powder coating reinforced with vinyltrimethoxysilane (VTMS)-functionalized ZrO₂ nanoparticles (V-ZrO₂) for thermal stability was developed. Chemical structure, microstructure and thermal degradation kinetics of the prepared coatings were investigated. The peak of aliphatic C–H vibrating bond in the Fourier transform infrared (FTIR) spectrum of V-ZrO₂ was a signature of VTMS attachment. Scanning electron microscopy (SEM) images revealed that, by increase of V-ZrO₂ content from 0.1 to 0.3 wt.% and then 0.5 wt.%, some agglomerations of nanoparticles are formed in the PU matrix. Thermogravimetric analysis (TGA) of the PU/V-ZrO₂ powder coatings was performed at different heating rates nonisothermally to capture alteration of activation energy (E_a) of degradation of PU/V-ZrO₂ powder coatings as a function of partial mass loss by using *Friedman*, *Kissinger–Akahira–Sunose (KAS)*, *Ozawa–Wall–Flynn (FWO)* and modified *Coats–Redfern* isoconversional approaches. It was observed that by addition of 1 wt.% V-ZrO₂ to PU resin the early state degradation temperature at 5% weight loss increased about 65 °C, suggesting a physical barrier effect limiting the volatility of free radicals and decomposition products. Incorporation of 5 wt.% ZrO₂ led to about 16% and 10% increase in E_a and LnA of blank PU, respectively, which was indicative of higher thermal resistance of nanocomposite powder coatings against thermal degradation. There was also obvious agreement between model outputs and experimental data. The results reveal that nanocomposite coating shows superior thermal properties compared to neat PU powder coatings, and the presence of nano ZrO₂ in sufficient amount causes retardation of the thermal decomposition process.

Keywords: polyurethane; powder coating; silane-functionalized ZrO₂ nanoparticles; thermogravimetric analysis; thermal degradation kinetics

1. Introduction

Fully solid, eco-friendly and cost-efficient are a number of characteristics that polyurethane (PU) thermoset powder coatings are known for among all the emerging coatings, and the reason why PU has been considered as the best alternative for construction and building materials to reduce the hazardous volatile organic chemicals quite frequently used in the paint and varnish industry [1,2]. The high cross-link density, energy saving features and excellent application performance have made PU coatings prominent candidates for decorative and protective purposes [3–6]. However, when it comes to the applications where stability and resistance to harsh conditions, such as thermal or stress shock, UV solar radiation and temperature elevations, are among the criteria, such coatings lose their properties as a consequence of cracking and thermal degradation that seriously shortens their service lifetime [7–9].

A common approach for improvement of polymer performance is to add a filler which can compensate for low properties of the matrix [10–13]. Accordingly, many studies have utilized this approach to modify the ultimate properties of the thermoset powder coatings. For example, Yu et al. [14] used CaCO₃ nanoparticles as a modifier in epoxy powder coatings and reported the remarkable enhancement in tensile property and corrosion resistance of the polymer. In the interest of modification of PU coatings' thermal properties, one should take advantage of nanoparticles that enhanced thermal stability and can retard the decomposition process of the polymer in harsh environments. Zirconium oxide (ZrO₂) nanostructures have proved good chemical resistance and mechanical properties as well as high resistance to thermal shock and low thermal conductivity [15]. Therefore, they are known as promising modifiers for thermal behavior of various kinds of polymers. Based on a thermal analysis conducted on ZrO₂/polyaniline nanocomposites, Wang et al. [16] have reported that the combination of these components resulted in higher thermal stability of the composites, which is ascribed to the matrix–filler interactions. Mishra et al. [17] have prepared nano-ZrO₂/polyether ether ketone (PEEK) nanocomposites and investigated the effect of the incorporation of this nanofiller on the thermal and mechanical properties. It was revealed that inclusion of nano-ZrO₂ in the matrix resulted in an enhanced thermal stability together with drastically increased mechanical features. In a recent study, an increased degradation temperature was reported for high density polyethylene (HDPE) nanocomposites of ZrO₂ nanomaterials [18]. In addition, scientists indicated that thermal protective performance of nano-ZrO₂/poly(ethylene oxide) (PEO) nanocomposites improves with an increase of nanoparticles concentration in the system [19]. Elsewhere, Reyes-Acosta et al. [20] introduced this nanomaterial to poly(methylmetacrylate)(PMMA) and reported improvement of mechanical properties and better UV protection compared to pure PMMA. Such behavior was ascribed to improved electrostatic polymer-nanoparticles interactions as well as radical trapping ability of ZrO₂ nanoparticles during the thermal degradation process of the matrix. Besides, they reported that the metal oxide nanoparticles tended to form agglomerations which adversely affected the transparency of the nanocomposite. As a result, it appears that surface modification of this nanomaterial can be as an effective method to further improve their performance as a modifier in polymeric matrices, since the hydroxyl groups on the surface of metal oxides prevents them being well-dispersed in non-hydrophilic media [21].

The complexity of PU thermal degradation necessitates a comprehensive investigation of decomposition/degradation kinetics of this polymer in order to optimize the formulation and processing conditions, as the basic requirements of high performance coatings [22]. Besides, addition of nanoparticles for improving the thermal stability of resins affects the kinetics of the reaction to help the coating survive in harsh conditions by the char formation mechanism [23–25]. As a result,

modelling of degradation reactions occurring in these systems would provide valuable information for better understanding of the role of each component, and obtaining a coating with improved thermal stability and properties as the ultimate goal [26].

In a previous work, isophorone diisocyanate 1,4-butanediol and 2-hydroxyethyl methacrylate were reacted to develop UV-curable urethane acrylate liquid resins [27]. Dibutyltin dilaurate was also added at specified amount to catalyze the reaction taking place in acetone as the media. UV-curable hybrid nanocomposite dispersions were developed by the addition of ZrO₂ nanoparticles varying ZrO₂-functionalized by vinyltrimethoxysilane (VTMS) coupling agent, as a potential formulation for UV-curable coatings. In this work, composites based on PU containing VTMS-functionalized ZrO₂ were formulated for powder coating application by addition of TiO₂, benzoin and baric at optimized contents, to develop nanocomposite powder coatings through processing with a twin screw extruder. Thermogravimetric analysis (TGA) was employed to investigate the effect of the ZrO₂ nanoparticles content on the thermal stability of polyurethane powder coatings. Besides, thermal degradation kinetics of ZrO₂/PU nanocomposites was modeled by the differential and integral isoconversional methods including *Friedman*, *Flynn–Wall–Ozawa (FWO)*, *Kissinger–Akahira–Sunose (KAS)*, and modified *Coats–Redfern (m-CR)*. The activation energy of decomposition reaction was also determined as a function of partial mass loss. Two models of n^{th} order and *Sestak–Berggren* were applied to predict the kinetic parameters of the reaction such as frequency factor and order of reaction. Eventually, the models were validated in comparison to experimental results.

2. Materials and Methods

2.1. Materials

Vinyltrimethoxysilane (VTMS) and isopropyl alcohol were supplied from Merck Co. (Darmstadt, Germany). Polyurethane powder coating resin and Vestagon B1530 hardener (Evonik Resource Efficiency GmbH, Marl, Germany) were formulated by Peka Chimie Co. (Tehran, Iran) and end product (9016 WU18AX) was used. Monoclinic crystal phase ZrO₂ spherical nanoparticles, with diameter of 40 nm and specific surface area of 20–40 m²·g⁻¹, was produced by US Research Nanomaterials Inc. (Houston, TX, USA). All the materials were used as received.

2.2. Sample Preparation

Nano ZrO₂ particles were chemically modified by silane coupling agent in isopropyl alcohol [27,28]. Then, the polyurethane powder coating was formulated with TiO₂, benzoin, baric and different amounts of modified nano ZrO₂ particles (1, 3 and 5 wt.%) were extruded in the twin-screw extruder (Yantai Donghui Powder Processing Equipment Company, Yantai, China). Thread diameter in this extruder was 20 mm with screw speed of 200 rpm. This device has three heating zones where the feeding zone was at temperature of 100 °C and the two others zone sets at 110 °C. The prepared chips were powdered and sieved to average particle size of 55 μm. The nanocomposite was electrostatically coated on 10 cm × 15 cm metal plates and cured at 180 °C for 15 min. The final nanocomposites were labeled as PU/V-ZrO₂-n, in which n shows the weight percent of nanoparticles present in the system.

2.3. Characterization

2.3.1. Fourier Transform Infrared Spectroscopy (FTIR) Analysis

VTMS modified ZrO₂ nanoparticles were characterized on a FTIR instrument of Spectrum one, PerkinElmer Inc., Boston, MA, USA. KBr pellet of the samples was prepared to collect FTIR spectra in a transmission mode within the wavelength range of 400–4000 cm⁻¹ with resolutions of 4 cm⁻¹.

2.3.2. Scanning Electron Microscopy (SEM)

The dispersion quality of VTMS-modified ZrO₂ nanoparticles in PU polymer matrix was observed using SEM. The micrographs were provided from the fractured surface of prepared PU nanocomposite powder coatings by Hitachi S-4160 SEM (Tokyo, Japan).

2.3.3. Thermal Decomposition Characterization

TGA analysis for each nanocomposite sample was conducted by Setaram Labsys Evo thermogravimetric analyzer (Setaram Labsys TM, Caluire, France). The first attempt prior to beginning the analysis, was drying of samples at 60 °C for 12 h to remove moisture. Afterwards, TGA measurement was performed on each sample under nitrogen atmosphere with fixed gas flow rate of 100 cm³·min⁻¹ in the temperature range of 25–600 °C at the heating rates of 5, 10 and 15 °C·min⁻¹.

2.4. Theoretical Background

One of the important parameters for studying the degradation behavior is the degree of degradation, or in other words, partial mass loss (α) which is expressed below [29]:

$$\alpha = \frac{(W_0 - W_t)}{(W_0 - W_f)}, \quad (1)$$

The thermal decomposition rate of the system can also be obtained by the following equation [30]:

$$\frac{d\alpha}{dt} = k(T)f(\alpha), \quad (2)$$

The $f(\alpha)$ in equation above is defined by the selected reaction model, while $k(T)$ is the reaction rate constant and follows the Arrhenius equation as below [31]:

$$k(T) = A \exp\left(-\frac{E_a}{RT}\right), \quad (3)$$

where A shows the pre-exponential factor, R is the universal gas constant and E_α indicates the activation energy of the thermal decomposition reactions.

Due to the intricacy of polymers decomposition process, a single equation cannot signify the mechanism by which the polymer degrades across the whole temperature range [32–35]. Therefore, the model-free isoconversional method comes forth to study this complicated procedure, according to which the temperature dependency of thermal decomposition rate function is considered at a constant degree of degradation. Based on the isoconversional methods, model-independent estimates of the activation energy (E_α) can be calculated. In this regard, two types of calculation methods can be applied to which are classified as differential and integral methods.

Speaking of differential methods, *Friedman* is considered to be the most common one due to its straightforward and approximation free method for evaluation of activation energy depending on the extent of reaction (α). By a simple rearrangement of Equations (2) and (3), *Friedman's* equation can be obtained as [36]:

$$\ln\left(\frac{d\alpha}{dt}\right) = \ln[Af(\alpha)] - \frac{E_\alpha}{RT}, \quad (4)$$

The activation energy can be calculated from the slope of the set of lines obtained through the plot of $\ln(d\alpha/dt)$ vs. $1/T$ at different heating rates and/or temperatures. It is noteworthy that this method may lead to erroneous results since TGA analysis result in integral data and applying differential method requires numerical differentiation which induces noise and inaccuracy to the final results and deviates the analysis from predicting the actual decomposition trend. As a result, the integral isoconversional methods are regarded as a higher priority for the thermal behavior study [37].

An advantageous integral method is *FWO* since it does not require a defined form of kinetic equation other than the Arrhenius temperature dependency and based on the Equation (5), the activation energy can be calculated from the slope of the plot of $\ln(\beta_i)$ vs. $1/T_\alpha$ at certain α at different heating rates [38]:

$$\ln(\beta_i) = Const - 1.052 \left(\frac{E_\alpha}{RT_\alpha} \right), \quad (5)$$

The crude temperature integral approximation in this method results in inaccurate values of E_α . A more accurate integral isoconversional method is the *KAS*, which can predict the activation energy of the degradation reaction through the slope of the curve of $\ln(\beta_i/T_{\alpha,i}^2)$ vs. $1/T$, as indicated in the following equation [39]:

$$\ln \left(\frac{\beta_i}{T_{\alpha,i}^2} \right) = Const - \left(\frac{E_\alpha}{RT_\alpha} \right), \quad (6)$$

Moreover, the *m-CR* method is used as the other isoconversional method to model the thermal degradation reaction [40]:

$$\ln \left[\frac{\beta}{T^2(1 - 2RT/E_\alpha)} \right] = \ln \left[\frac{-AR}{E_\alpha \ln(1 - \alpha)} \right] - \frac{E_\alpha}{RT}, \quad (7)$$

Based on Equation (7), one can obtain a straight line by plotting $\ln[\beta/T^2(1 - 2RT/E_\alpha)]$ against $1/T$, the slope of which gives the activation energy of degradation reaction. The E_α values that obtained from *Friedman*, *KAS* and *FWO* methods can be used as a first guess for iterative method to reach the complete solution of Equation (7).

The reaction kinetics comprehension cannot be fulfilled until the dependency of a reaction is represented as a function of reaction progress. For instance, the simplest prediction model for such processes can be defined as following n^{th} order decomposition reactions [41,42]:

$$f(\alpha) = (1 - \alpha)^n, \quad (8)$$

In cases where the reactions are more complex, such as autocatalytic ones, the *Sestak* and *Berggren* (*SB*) [43] empirical kinetic model can be proposed:

$$f(\alpha) = \alpha^m(1 - \alpha)^n, \quad (9)$$

3. Results

Figure 1 shows the FTIR spectra of ZrO_2 - and VTMS-modified ZrO_2 nanoparticles. Zr–O bonds existing in the chemical structure of nanoparticles appeared at the wavenumbers of 500, 671 and 749 cm^{-1} . The band at 3401 cm^{-1} is ascribed to the hydroxyl stretching vibration of absorbed moisture. When the nanoparticle is modified by VTMS molecules, the bands attributed to Si–O–Zr and $\text{CH}_3\text{--Si(O--)}_3$ are overlapping, and can be observed in the range of 550–950 cm^{-1} as a wide peak as well as the band at 1135 cm^{-1} which show Si–O–Si bond. The peak at 1409 cm^{-1} indicates the dual bond introduced to the system (Si–CH=CH₂). The small peaks that appeared at 3021 and 3061 cm^{-1} confirm the presence of symmetric and asymmetric C–H bonds, respectively. As a result, the modification process of ZrO_2 nanoparticles with VTMS molecules is confirmed.

Figure 2 represents the state of dispersion in the blank and nanocomposite PU samples at different concentrations of the filler. Observing the SEM graphs meticulously, one can realize that the dispersion and distribution of nanoparticles in PU, specifically at the lowest loading, are uniform so that the resin wets the nanoparticles properly. This can be ascribed to the carbon dual bond (C=C) in the VTMS structure that can radically polymerize with polyurethane end groups and interacts physically with the polymer [21]. As the concentration of the filler increases, a few agglomerations appear in the PU matrix which can affect the final properties.

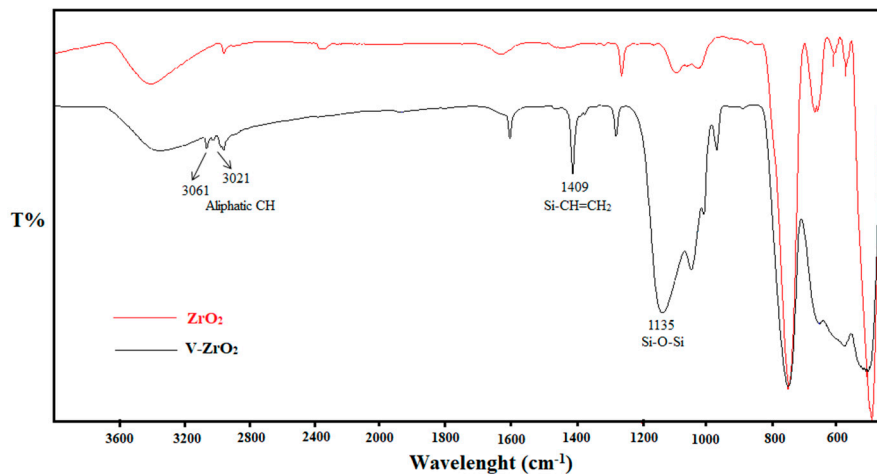


Figure 1. FTIR spectra of ZrO_2 and $V-ZrO_2$ [27].

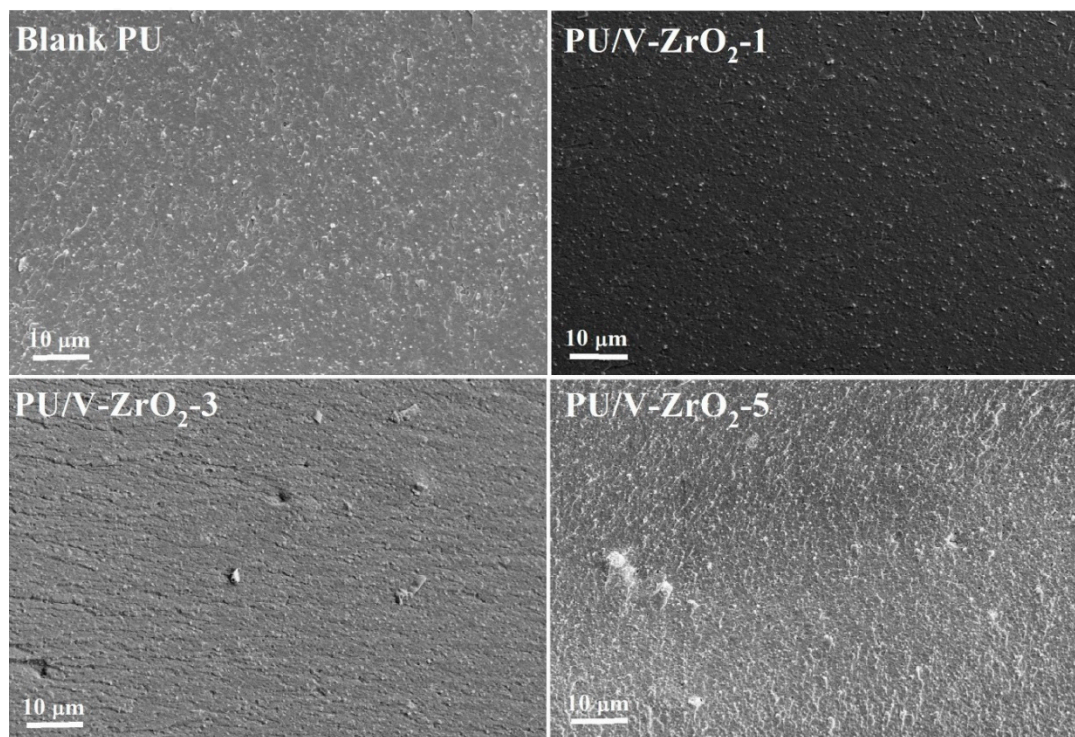


Figure 2. SEM micrographs of blank polyurethane (PU) and its nanocomposites containing 1, 3 and 5 wt.% of $V-ZrO_2$, such that by increase of $V-ZrO_2$ content, from 0.1 to 0.3 wt.% and then 0.5 wt.%, some agglomerations of nanoparticles can be observed in the PU matrix.

To track the participation of ZrO_2 nanoparticles in the thermal stability of PU, TGA measurement was conducted on the blank PU and all the nanocomposites samples. As the thermograms demonstrate in the Figure 3, the main decomposition process of PU happens above the temperature of 200 °C. A slight mass loss occurring at around 150 °C can be attributed to evaporation of moisture and volatile molecules absorbed during the processing of samples. The sharp mass loss starting at 350 °C shows the main decomposition reaction of the system.

The thermal decomposition characteristic of samples can be calculated based on the data obtained from TGA measurements, which is reported in Table 1. Compared to pure PU, introduction of ZrO_2 nanostructures caused remarkable rise in the temperature of 5% and 10% mass loss ($T_{5\%}$ and $T_{10\%}$). This reveals the physical barrier effect of the nanoparticles against emission of volatile compounds

generated from decomposition processes, and also the strong interaction between modified particles and the matrix. However, this trend is not followed for the nanocomposites with highest content of nanoparticles, due to aggregation of the filler particles, which leads to void formation. Moreover, the residual char content at 600 °C shows that thermally stable nanoparticles of nano-ZrO₂ play a pivotal role in improving the PU polymer in order to reach thermal stability at high temperatures. The metal cations help the formation of double bonds, capable of cross-linking, which facilitates the char formation at high temperatures [44]. Besides, the double bond provided in the system thanks to VTMS modification further boosts this process. The results from DTG curve indicates that the rate of decomposition increases by further loading of nanoparticles, except for the nanocomposite with 1 wt.% ZrO₂ which showed lower residual content as well. This behavior implies that metal oxides can catalyze the chain scission reactions, as it is previously reported in the literature [45].

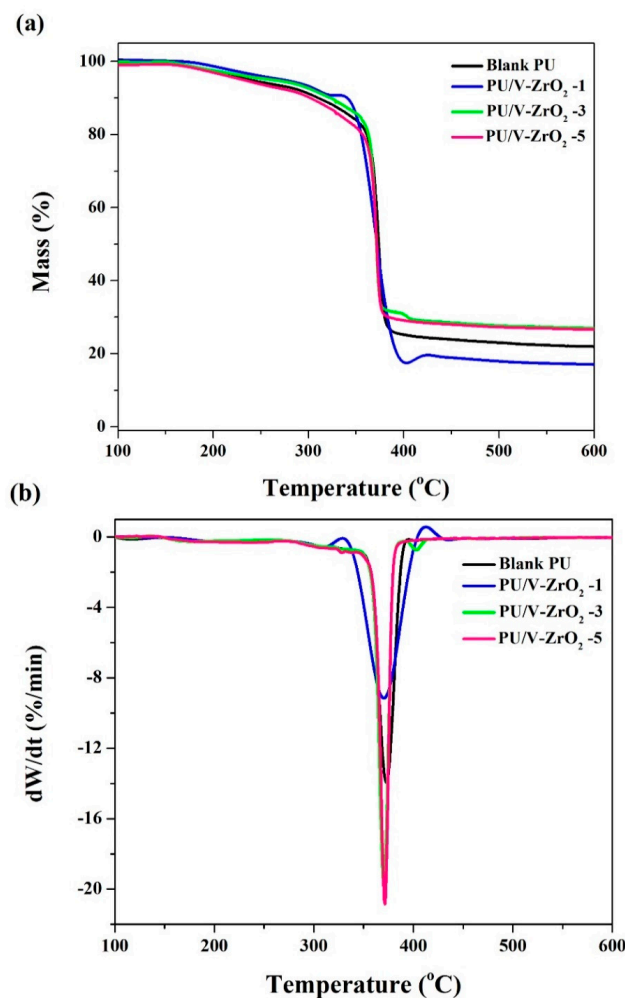


Figure 3. (a) Thermo Gravimetric Analysis (TGA) and (b) Derivative Thermogravimetric Analysis (DTGA) thermograms of PU/ V-ZrO₂ nanocomposites at $\beta = 5 \text{ }^\circ\text{C}\cdot\text{min}^{-1}$.

Table 1. Thermal decomposition characteristics of PU/V-ZrO₂ nanocomposites derived from TGA diagrams at $\beta = 5 \text{ }^\circ\text{C}\cdot\text{min}^{-1}$.

Designation	T _{5%} (°C)	T _{10%} (°C)	T _P (°C)	Residue (%)
Blank	237.47	309.60	372.86	21.09
ZrO ₂ -1	272.60	340.83	370.16	17.11
ZrO ₂ -3	261.78	323.24	370.47	27.04
ZrO ₂ -5	230.80	301.86	371.45	26.64

It can be realized that, at lower concentrations, low amounts of nanoparticles in the system is able to take part in the first stage of the PU decomposition process, which is related to the hard segments of polyurethane. On the other hand, the higher amounts of nano-ZrO₂ cannot enhance the thermal features of polymer at lower temperatures, and its role is highlighted at the later stage of degradation process associated to the soft segments and char formation at elevated temperatures.

The calculated conversion (α) as a function of temperature is presented in Figure 4, in which the blank sample and each of the V-ZrO₂ nanocomposites of epoxy are shown at three different heating rates. It is realized that the heating rate can affect the pyrolysis process greatly, since at higher heating rates the pyrolysis progress is accelerated and the reaction temperature window is shifted to the higher temperatures. This is a trend that is observed for all the samples, demonstrating that, regardless of the amount of nanoparticles, the pyrolysis reaction is dependent on the heating rates.

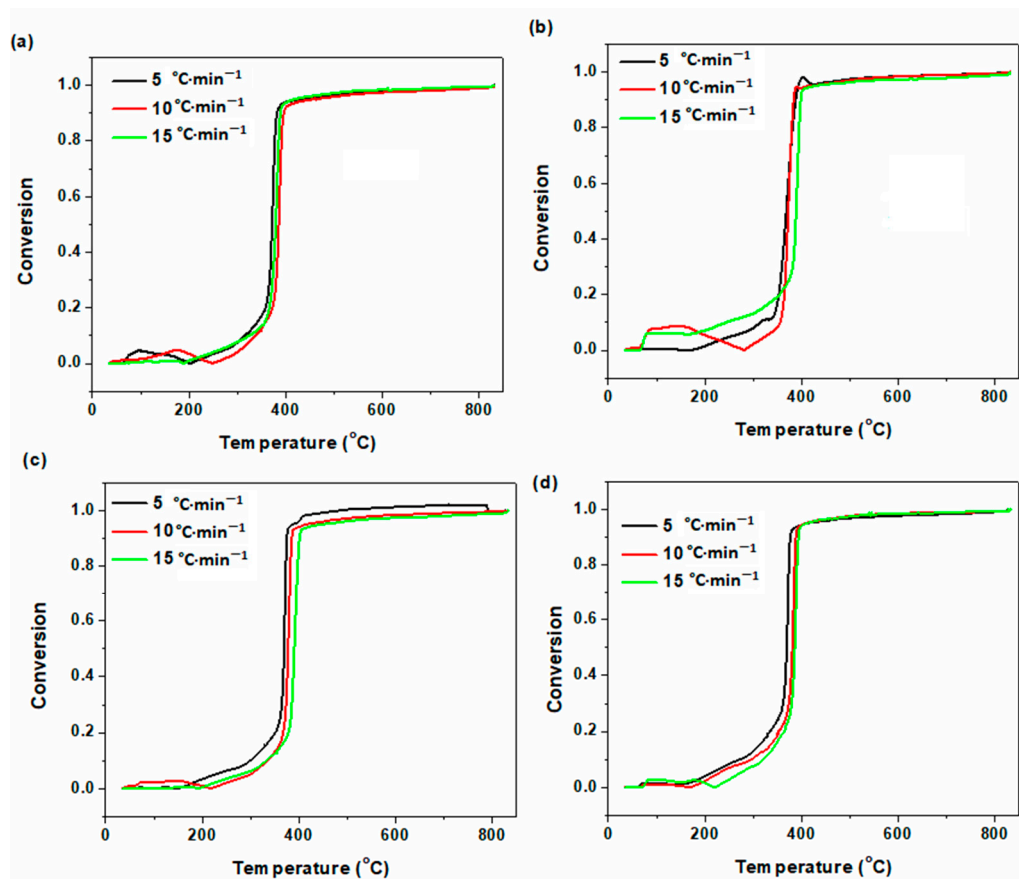


Figure 4. Degradation conversion profiles at various heating rates for (a) blank PU, (b) PU/V-ZrO₂-1, (c) PU/V-ZrO₂-3 and (d) PU/V-ZrO₂-5.

The results of the calculations based on isoconversional methods are represented in Figure 5. It is obvious that the differential *Friedman* method is not compatible with the integral method of TGA and could not predict the degradation behavior accurately. The three other methods produced almost parallel lines in the α range between 0.3 to 0.9, which is indicative of a decomposition kinetic with a single mechanism for PU/V-ZrO₂ nanocomposites [46].

The variation of activation energy of thermal decomposition reactions, which was obtained based on isoconversional methods, is demonstrated in Figure 6 with respect to partial mass loss of blank PU and its ZrO₂ nanocomposites. The similar trend and almost similar values of activation energy obtained by *KAS*, *FWO* and *m-CR* isoconversional methods indicates that these three models are able to predict the decomposition behavior more accurately. However, the *Friedman* method encounters oscillation especially at low conversion, whereby the equipment sensitivity causes data deviation

and instability [30]. Generally, the presence of ZrO₂ nanoparticles decreased the activation energy of decomposition process at early stages (before $\alpha = 0.3$), which can be attributed to the unstable bonds and weak links that facilitate the degradation reaction. Subsequently, the activation energy of nanocomposites is almost equal to the blank sample except for the nanocomposite with the highest loading of ZrO₂ nanoparticles. Higher amount of thermally-stable ZrO₂ nanoparticles in the PU matrix makes the mobility of soft PU chains constrained, leading to the higher activation energy values. The V-ZrO₂ surface can interact physically with the PU matrix, which is shown schematically in Figure 7. In addition, it can be found that a sufficient amount of ZrO₂ nanoparticles increases the difficulty for the reaction to progress, which is implied as a higher thermal stability and denser PU 3D network.

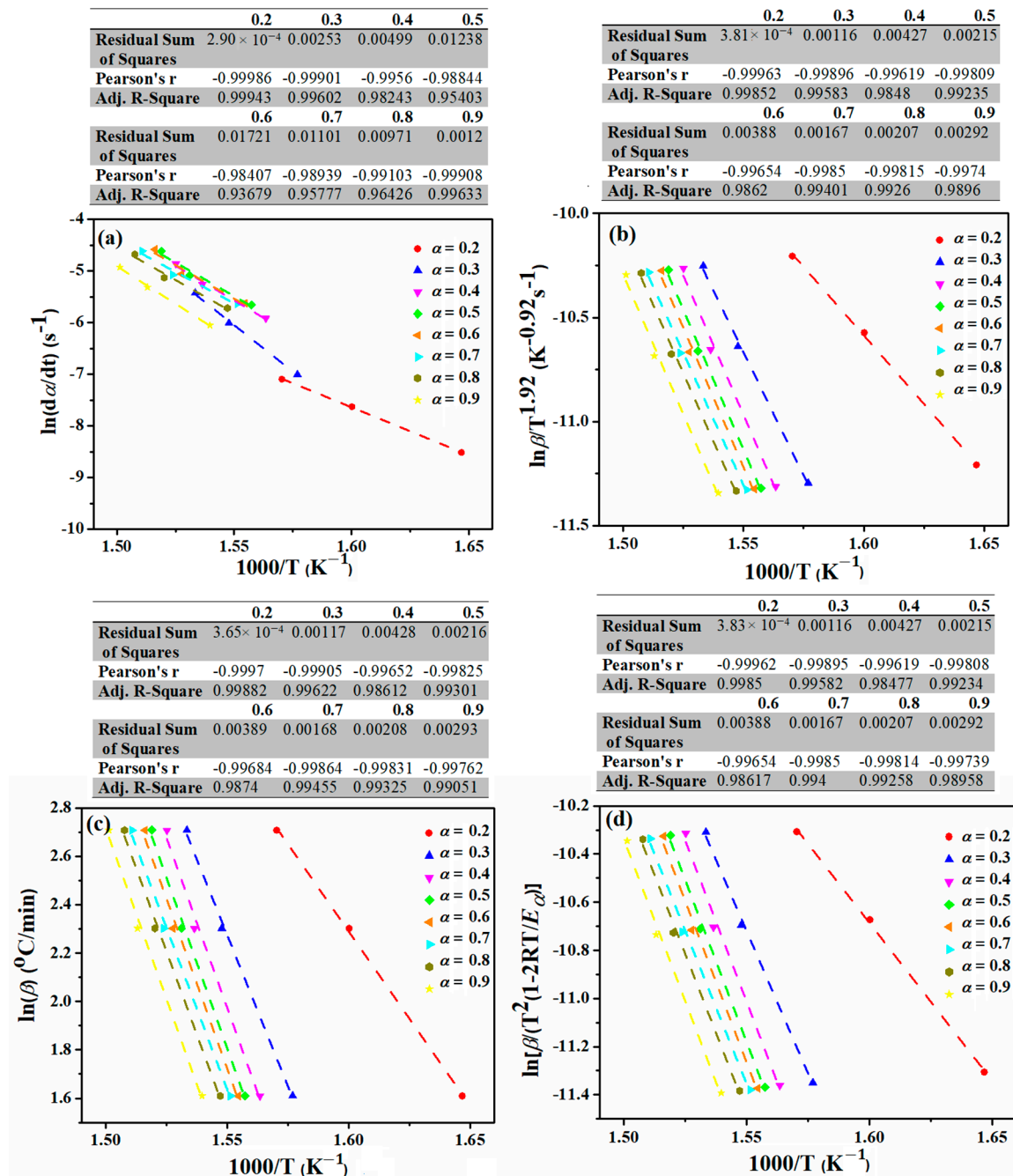


Figure 5. Typical isoconversional plots for PU/V-ZrO₂ nanocomposites (a) Friedman, (b) Kissinger-Akahira-Sunose (KAS), (c) Ozawa-Wall-Flynn (FWO) and (d) modified Coats-Redfern (m-CR) methods.

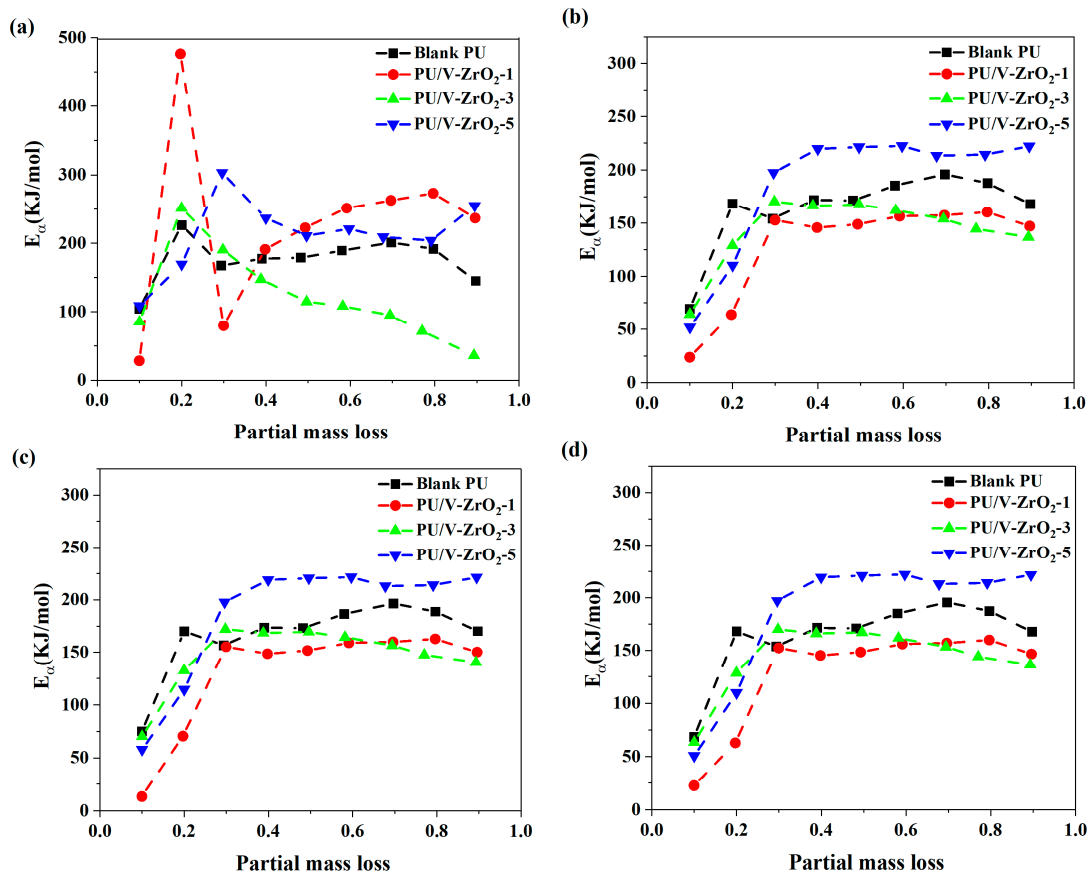


Figure 6. Activation energy of blank PU and its nanocomposites containing 1, 3 and 5 wt.% of V-ZrO₂ nanoparticles in terms of partial mass loss obtained using (a) Friedman (b) KAS, (c) FWO and (d) *m*-CR methods.

Based on Equation (8), the kinetic parameters of activation energy E_{α} , pre-exponential factor $\ln(A)$ and decomposition reaction order n are calculated for all the blank and nanocomposite samples, the results of which are listed in Table 2. Likewise, the values of two kinetic exponents (m , n) as well as other parameters of E_{α} and A are provided in Table 3.

A decrease in n value, decomposition reaction order, is resulted by the introduction of V-ZrO₂ nanoparticles to the PU matrix. Basically, the drop in the reaction order shows the reaction was slowed down and its rate decreased. However, one can observe that for the PU/V-ZrO₂ nanocomposite with the ZrO₂ nanoparticles concentration of 0.3 wt.%, the reaction order raised up to the one for blank sample. This behavior can be attributed to the role of such concentration in this phenomenon. The nanoparticles at the lower concentration can be distributed more uniformly and the high interfacial surface between the nanoparticles and matrix hardens the molecular motion and decrease the decomposition rate. This is also the case for the nanocomposite with highest loading, which causes the higher amounts of highly stable nanomaterial in the system, and thereby higher probability of the reaction due to the numerous functionalities existing in the system. This behavior is also observed for the results acquired by the SB method and it can be seen that both n and m parameters reach the values as high as the ones for blank PU.

Moreover, it is proposed that frequency factor of A is directly dependent on E_{α} [47] and a rise in A is equivalent to the increase of E_{α} . This parameter is a measure of the rate of components vibration in the system. By evaluating the results of Tables 2 and 3, the dependency of A and E_{α} is revealed. As mentioned above, the activation energy and, consequently, the frequency factor for nanocomposite of 1 and 3 wt.% ZrO₂ are scaled down due to the unstable bonds present in the system. On the other hand, for the proper amount of nanoparticle (5 wt.%), the polymer chains can dissipate more energy

and resist against thermal decomposition. It is worth to mention that values calculated based on different integral isoconversional methods are equal with a good approximation.

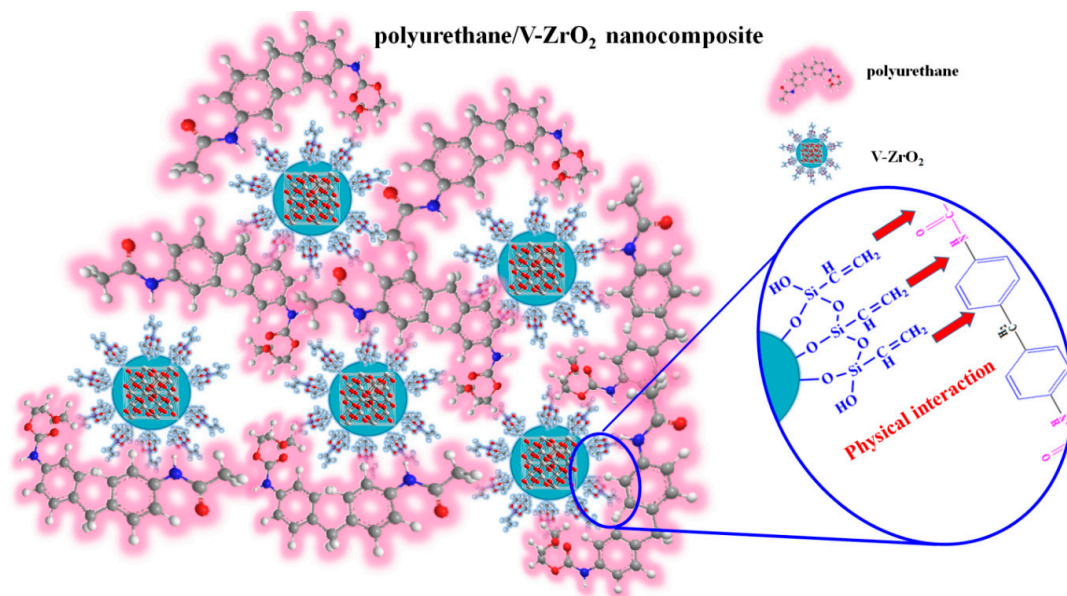


Figure 7. Typical interaction and dispersion state of V-ZrO₂ nanoparticles in PU matrix.

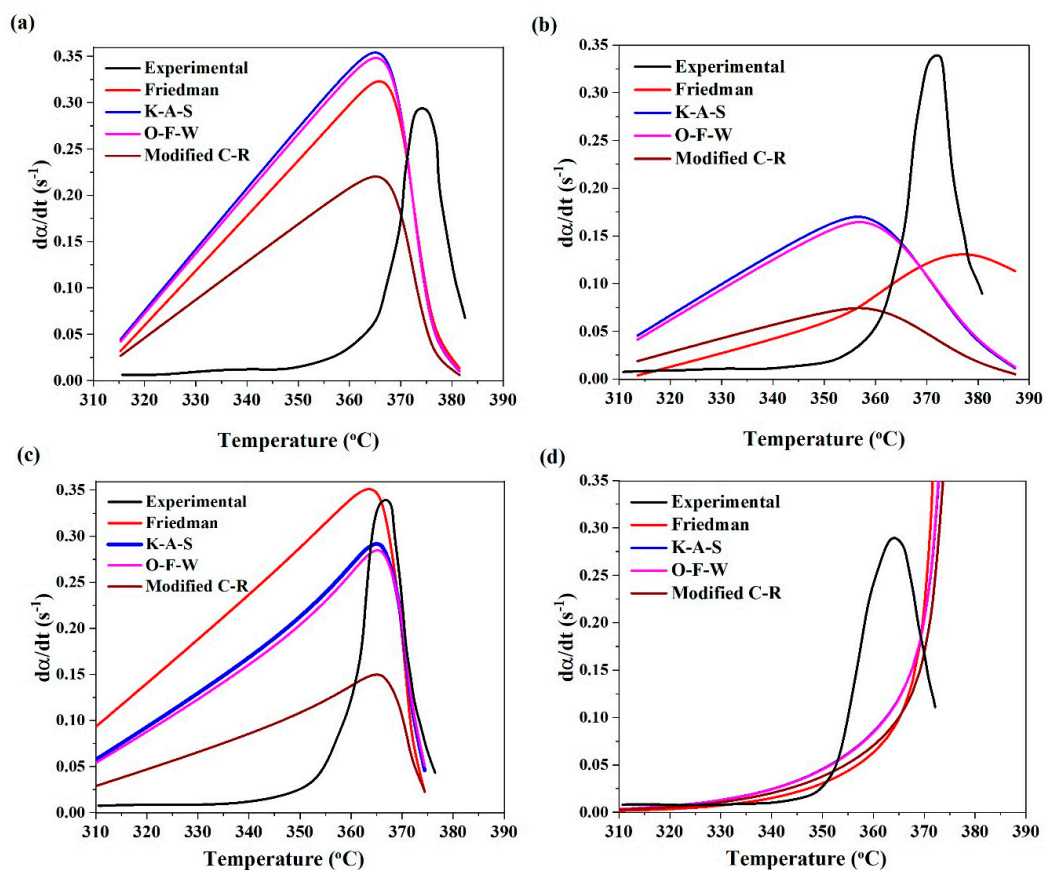
Table 2. Decomposition parameters based on the n^{th} order decomposition reaction of PU and PU nanocomposites calculated using different isoconversional kinetic models.

	Designation	Blank	ZrO ₂ -1	ZrO ₂ -3	ZrO ₂ -5
Friedman	E_{α} (kJ·mol ⁻¹)	184.67	249.33	126.81	226.23
	$Ln A$ (min ⁻¹)	38.12	46.57	27.55	43.66
	n	7.22	2.93	7.03	3.89
KAS	E_{α} (kJ·mol ⁻¹)	175.38	141.58	153.84	202.58
	$Ln A$ (min ⁻¹)	36.42	26.47	32.43	39.58
	n	7.26	3.00	6.78	4.38
FWO	E_{α} (kJ·mol ⁻¹)	177.01	144.88	156.54	202.79
	$Ln A$ (min ⁻¹)	36.71	27.08	32.92	39.61
	n	7.25	3.00	6.75	4.37
m -CR	E_{α} (kJ·mol ⁻¹)	175.02	141.08	153.42	202.26
	$Ln A$ (min ⁻¹)	36.35	26.37	32.35	39.52
	n	7.26	3.00	6.78	4.39

A common approach to validate the predicted values by n^{th} order and SB models is to plot the rate of decomposition reaction as a function of temperature for the experimental and theoretical data. Figures 8 and 9 demonstrate the related plots obtained by n^{th} order and SB model, respectively, for blank PU and its nanocomposites of ZrO₂ nanoparticles. Based on Figure 8, the n^{th} order model is not capable of predicting the trend of experimental model and shows deviations. However, this model can only predict the early or late stage of the reaction in 3 and 5 wt.% PU/ZrO₂ nanocomposites, respectively. On the contrary, the results of Figure 9 indicate that the two kinetic exponents of SB model are more accurately correlated to the experimental data. However, the m -CR method is behaving different in comparison to other integral methods and even differential method of *Friedman*. It is evident that the greater the content of V-ZrO₂ in the system, the greater the number of deviations that appear from the experimental data.

Table 3. Decomposition parameters based on the Sestak and Berggren decomposition reaction of PU nanocomposites calculated using different isoconversional kinetic models.

Designation		Blank	ZrO ₂ -1	ZrO ₂ -3	ZrO ₂ -5
Friedman	E_{α} (kJ·mol ⁻¹)	184.67	249.33	126.81	226.23
	$Ln A$ (min ⁻¹)	38.12	46.57	27.55	43.66
	m	3.55	0.77	3.96	1.96
	n	3.68	2.16	3.07	1.93
KAS	E_{α} (kJ·mol ⁻¹)	175.38	141.58	153.84	202.58
	$Ln A$ (min ⁻¹)	36.42	26.47	32.43	39.58
	m	3.58	1.12	3.79	2.28
	n	3.68	1.88	2.99	2.10
FWO	E_{α} (kJ·mol ⁻¹)	177.01	144.88	156.54	202.79
	$Ln A$ (min ⁻¹)	36.71	27.08	32.92	39.61
	m	3.58	1.11	3.77	2.27
	n	3.68	1.89	2.99	2.10
m-CR	E_{α} (kJ·mol ⁻¹)	175.02	141.08	153.42	202.26
	$Ln A$ (min ⁻¹)	36.35	26.37	32.35	39.52
	m	3.58	1.11	3.78	2.28
	n	3.68	1.89	3.00	2.11

**Figure 8.** Predicted kinetics plots based on the n^{th} order decomposition reaction model for blank PU and its nanocomposites containing various V-ZrO₂ loadings at the heating rate of 5 °C·min⁻¹: (a) Blank PU; (b) PU/V-ZrO₂-1; (c) PU/V-ZrO₂-3; and (d) PU/V-ZrO₂-5.

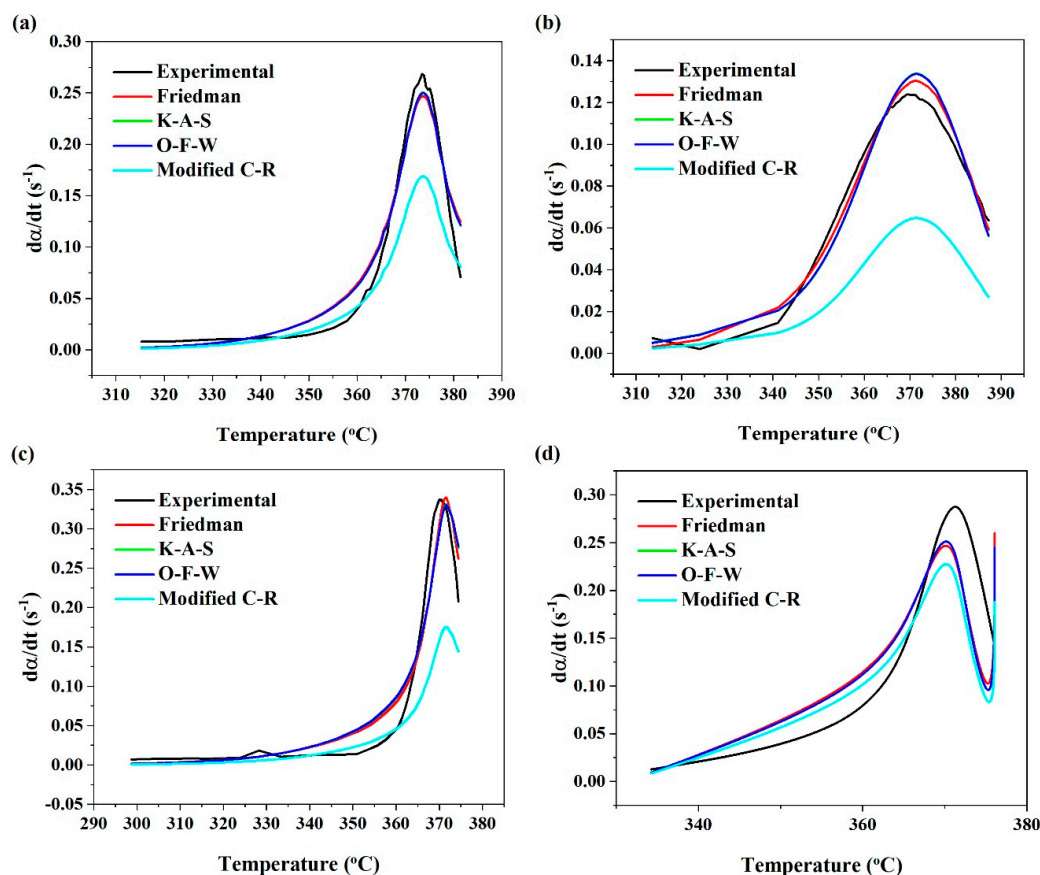


Figure 9. Predicted kinetics plots based on the Sestak and Berggren decomposition reaction model for blank PU and its nanocomposites containing various V-ZrO₂ loadings at the heating rate of 5 °C·min⁻¹: (a) Blank PU; (b) PU/V-ZrO₂-1; (c) PU/V-ZrO₂-3; and (d) PU/V-ZrO₂-5.

4. Conclusions

Polyurethane decomposition kinetics in the presence of various amounts (1, 3 and 5 wt.%) of VTMS-modified ZrO₂ nanoparticles (V-ZrO₂) was studied by TGA analysis and different model-free isoconversional methods (differential and integral), including *Friedman*, *FWO*, *KAS* and *m-CR*, were applied to predict activation energy and other kinetic parameters as a function of partial mass loss. It was observed that by introduction of 1 wt.% ZrO₂ nanoparticles to PU resin, the T_{5%} of the nanocomposite increased about 65 °C, indicating the physical barrier effect, limiting the volatility of free radicals and decomposition products. Further addition of nanoparticles caused a decreasing trend in T_{5%}, which can be attributed to the void formation as a result of nanoparticles aggregation. The activation energy calculated based on isoconversional methods showed that the values are strongly dependent on the nanoparticles concentration. For low concentrations of ZrO₂ nanoparticles in the system, E_α was decreased to values lower than the blank sample, which was ascribed to facilitated reaction due to presence of weak links and unstable bonds. However, the sufficient amount of thermally-stable nanoparticles (PU/V-ZrO₂-5) caused a 25 °C rise in the activation energy value compared to the reference sample, which reveals that polymer chains dissipate more energy and are more resistant to the elevated temperatures. The differential method of *Friedman* was not capable of providing the precise estimation of the reaction characteristics and showed more deviation compared to other applied models. The *Sestak* and *Berggren* model could better predict and represent the decomposition process of PU and its nanocomposites of V-ZrO₂. In conclusion, it can be acclaimed that the novel nanocomposite coating prepared in this work reveals improved thermal resistance and stability pertinent to the amounts of modified nanoparticles present in the system. The ZrO₂

nanoparticles retard the decomposition process of the coating and prolong its lifetime at extreme thermal conditions.

Author Contributions: Conceptualization, M.R.S.; methodology, B.S.H. and M.J.; software, S.M.R.P.; validation, M.J. and H.V.; formal analysis, H.F.B.; investigation, M.J. and H.H.; data curation, M.J. and S.M.R.P.; writing—original draft preparation, F.T.; writing—review and editing, K.F., A.E. and A.M.; visualization, H.V.; supervision, M.R.S.; All authors have read and agreed to the published version of the manuscript.

Funding: This research received no external funding.

Conflicts of Interest: The authors declare no conflict of interest.

References

1. Spyrou, E.; Loesch, H.; Wenning, A. Low-Temperature-Curable, Solid Polyurethane Powder Coating Compositions Containing Uretdione Groups. U.S. Patent 6914115, 5 July 2005.
2. Schmitt, F.; Wenning, A.; Weiss, J.-V. Dimeric isocyanates in polyurethane powder coatings. *Prog. Org. Coat.* **1998**, *34*, 227–235. [[CrossRef](#)]
3. Sultan, M.; Atta, S.; Bhatti, H.N.; Islam, A.; Jamil, T.; Bibi, I.; Gull, N. Synthesis, characterization, and application studies of polyurethane acrylate thermoset coatings: Effect of hard segment. *Polym. Plast. Technol. Eng.* **2017**, *56*, 1608–1618. [[CrossRef](#)]
4. Lee, S.S.; Han, H.Z.; Hilborn, J.G.; Månson, J.-A.E. Surface structure build-up in thermosetting powder coatings during curing. *Prog. Org. Coat.* **1999**, *36*, 79–88. [[CrossRef](#)]
5. Visakh, P.; Semkin, A.; Rezaev, I.; Fateev, A. Review on soft polyurethane flame retardant. *Constr. Build. Mater.* **2019**, *227*, 116673. [[CrossRef](#)]
6. Zhang, Z.; Sun, J.; Jia, M.; Qi, B.; Zhang, H.; Lv, W.; Mao, Z.; Chang, P.; Peng, J.; Liu, Y. Study on a thermosetting polyurethane modified asphalt suitable for bridge deck pavements: Formula and properties. *Constr. Build. Mater.* **2020**, *241*, 118122. [[CrossRef](#)]
7. Rossi, S.; Fedel, M.; Petrolli, S.; Deflorian, F. Accelerated weathering and chemical resistance of polyurethane powder coatings. *J. Coat. Technol. Res.* **2016**, *13*, 427–437. [[CrossRef](#)]
8. Chen, B.; He, M.; Huang, Z.; Wu, Z. Long-term field test and numerical simulation of foamed polyurethane insulation on concrete dam in severely cold region. *Constr. Build. Mater.* **2019**, *212*, 618–634. [[CrossRef](#)]
9. Somarathna, H.; Raman, S.N.; Mohotti, D.; Mutalib, A.A.; Badri, K. The use of polyurethane for structural and infrastructural engineering applications: A state-of-the-art review. *Constr. Build. Mater.* **2018**, *190*, 995–1014. [[CrossRef](#)]
10. Aliakbari, M.; Jazani, O.M.; Sohrabian, M.; Jouyandeh, M. Multi-nationality epoxy adhesives on trial for future nanocomposite developments. *Prog. Org. Coat.* **2019**, *133*, 376–386. [[CrossRef](#)]
11. Jouyandeh, M.; Rahmati, N.; Movahedifar, E.; Hadavand, B.S.; Karami, Z.; Ghaffari, M.; Taheri, P.; Bakhshandeh, E.; Vahabi, H.; Ganjali, M.R. Properties of nano-Fe₃O₄ incorporated epoxy coatings from Cure Index perspective. *Prog. Org. Coat.* **2019**, *133*, 220–228. [[CrossRef](#)]
12. Akbari, V.; Najafi, F.; Vahabi, H.; Jouyandeh, M.; Badawi, M.; Morisset, S.; Ganjali, M.R.; Saeb, M.R. Surface chemistry of halloysite nanotubes controls the curability of low filled epoxy nanocomposites. *Prog. Org. Coat.* **2019**, *135*, 555–564. [[CrossRef](#)]
13. Karami, Z.; Jouyandeh, M.; Ali, J.A.; Ganjali, M.R.; Aghazadeh, M.; Paran, S.M.R.; Naderi, G.; Puglia, D.; Saeb, M.R. Epoxy/layered double hydroxide (LDH) nanocomposites: Synthesis, characterization, and Excellent cure feature of nitrate anion intercalated Zn-Al LDH. *Prog. Org. Coat.* **2019**, *136*, 105218. [[CrossRef](#)]
14. Yu, H.; Wang, L.; Shi, Q.; Jiang, G.; Zhao, Z.; Dong, X. Study on nano-CaCO₃ modified epoxy powder coatings. *Prog. Org. Coat.* **2006**, *55*, 296–300. [[CrossRef](#)]
15. Wang, P.; Ma, Q.; Li, B.; Li, Y. Microstructure and Thermal-protective Property of CPED Coating with ZrO₂ Nanoparticles Addition on Al-12Si Alloy. *J. Wuhan Univ. Technol. Mater. Sci. Ed.* **2019**, *34*, 1187–1192. [[CrossRef](#)]
16. Wang, S.; Tan, Z.; Li, Y.; Sun, L.; Zhang, T. Synthesis, characterization and thermal analysis of polyaniline/ZrO₂ composites. *Thermochim. Acta* **2006**, *441*, 191–194. [[CrossRef](#)]
17. Mishra, T.; Kumar, A.; Verma, V.; Pandey, K.; Kumar, V. PEEK composites reinforced with zirconia nanofiller. *Compos. Sci. Technol.* **2012**, *72*, 1627–1631. [[CrossRef](#)]

18. Nabiyev, A.; Olejniczak, A.; Pawlukoje, A.; Balasoju, M.; Bunoiu, M.; Maharramov, A.; Nuriyev, M.; Ismayilova, R.; Azhibekov, A.; Kabyshev, A. Nano-ZrO₂ filled high-density polyethylene composites: Structure, thermal properties, and the influence γ -irradiation. *Polym. Degrad. Stab.* **2020**, *171*, 109042. [[CrossRef](#)]
19. Wang, P.; Han, J.; Yan, J.; Wang, J. Effects of ZrO₂ Nanoparticles on the Microstructure and Thermal-protective Properties of PEO Coating on Al-12.5% Si Alloy. *J. Wuhan Univ. Technol. Mater. Sci. Ed.* **2019**, *34*, 156–164. [[CrossRef](#)]
20. Reyes-Acosta, M.; Torres-Huerta, A.M.; Dominguez-Crespo, M.A.; Flores-Vela, A.I.; Dorantes-Rosales, H.J.; Ramírez-Meneses, E. Influence of ZrO₂ nanoparticles and thermal treatment on the properties of PMMA/ZrO₂ hybrid coatings. *J. Alloys Compd.* **2015**, *643*, S150–S158. [[CrossRef](#)]
21. Sow, C.; Riedl, B.; Blanchet, P. UV-waterborne polyurethane-acrylate nanocomposite coatings containing alumina and silica nanoparticles for wood: Mechanical, optical, and thermal properties assessment. *J. Coat. Technol. Res.* **2011**, *8*, 211–221. [[CrossRef](#)]
22. Ma, X.; Tu, R.; Ding, C.; Zeng, Y.; Wang, Y.; Fang, T. Thermal and fire risk analysis of low pressure on building energy conservation material flexible polyurethane with various inclined facade constructions. *Constr. Build. Mater.* **2018**, *167*, 449–456. [[CrossRef](#)]
23. Vahabi, H.; Jouyandeh, M.; Cochez, M.; Khalili, R.; Vagner, C.; Ferriol, M.; Movahedifar, E.; Ramezanzadeh, B.; Rostami, M.; Ranjbar, Z. Short-lasting fire in partially and completely cured epoxy coatings containing expandable graphite and halloysite nanotube additives. *Prog. Org. Coat.* **2018**, *123*, 160–167. [[CrossRef](#)]
24. Saeb, M.; Vahabi, H.; Jouyandeh, M.; Movahedifar, E.; Khalili, R. Epoxy-based flame retardant nanocomposite coatings: Comparison between functions of expandable graphite and halloysite nanotubes. *Prog. Colorcolorants Coat.* **2017**, *10*, 245–252.
25. Yuan, H.; Shi, Y.; Xu, Z.; Lu, C.; Ni, Y.; Lan, X. Influence of nano-ZrO₂ on the mechanical and thermal properties of high temperature cementitious thermal energy storage materials. *Constr. Build. Mater.* **2013**, *48*, 6–10. [[CrossRef](#)]
26. Paran, S.M.R.; Vahabi, H.; Jouyandeh, M.; Ducos, F.; Formela, K.; Saeb, M.R. Thermal decomposition kinetics of dynamically vulcanized polyamide 6-acrylonitrile butadiene rubber-halloysite nanotube nanocomposites. *J. Appl. Polym. Sci.* **2019**, *136*, 47483. [[CrossRef](#)]
27. Madhi, A.; Shirkavand Hadavand, B.; Amoozadeh, A. UV-curable urethane acrylate zirconium oxide nanocomposites: Synthesis, study on viscoelastic properties and thermal behavior. *J. Compos. Mater.* **2018**, *52*, 2973–2982. [[CrossRef](#)]
28. Hadavand, B.S.; Ataefard, M.; Bafghi, H.F. Preparation of modified nano ZnO/polyester/TGIC powder coating nanocomposite and evaluation of its antibacterial activity. *Compos. Part B Eng.* **2015**, *82*, 190–195. [[CrossRef](#)]
29. Bockhorn, H.; Hornung, A.; Hornung, U. Mechanisms and kinetics of thermal decomposition of plastics from isothermal and dynamic measurements. *J. Anal. Appl. Pyrolysis* **1999**, *50*, 77–101. [[CrossRef](#)]
30. Yao, F.; Wu, Q.; Lei, Y.; Guo, W.; Xu, Y. Thermal decomposition kinetics of natural fibers: Activation energy with dynamic thermogravimetric analysis. *Polym. Degrad. Stab.* **2008**, *93*, 90–98. [[CrossRef](#)]
31. Jouyandeh, M.; Paran, S.M.R.; Shabaniyan, M.; Ghiyasi, S.; Vahabi, H.; Badawi, M.; Formela, K.; Puglia, D.; Saeb, M.R. Curing behavior of epoxy/Fe₃O₄ nanocomposites: A comparison between the effects of bare Fe₃O₄, Fe₃O₄/SiO₂/chitosan and Fe₃O₄/SiO₂/chitosan/imide/phenylalanine-modified nanofillers. *Prog. Org. Coat.* **2018**, *123*, 10–19. [[CrossRef](#)]
32. Rastin, H.; Saeb, M.R.; Nonahal, M.; Shabaniyan, M.; Vahabi, H.; Formela, K.; Gabrion, X.; Seidi, F.; Zarrintaj, P.; Sari, M.G.; et al. Transparent nanocomposite coatings based on epoxy and layered double hydroxide: Nonisothermal cure kinetics and viscoelastic behavior assessments. *Prog. Org. Coat.* **2017**, *113*, 126–135. [[CrossRef](#)]
33. Saeb, M.R.; Rastin, H.; Shabaniyan, M.; Ghaffari, M.; Bahlakeh, G. Cure kinetics of epoxy/ β -cyclodextrin-functionalized Fe₃O₄ nanocomposites: Experimental analysis, mathematical modeling, and molecular dynamics simulation. *Prog. Org. Coat.* **2017**, *110*, 172–181. [[CrossRef](#)]
34. Saeb, M.R.; Nonahal, M.; Rastin, H.; Shabaniyan, M.; Ghaffari, M.; Bahlakeh, G.; Ghiyasi, S.; Khonakdar, H.A.; Goodarzi, V.; Vijayan, P.P.; et al. Calorimetric analysis and molecular dynamics simulation of cure kinetics of epoxy/chitosan-modified Fe₃O₄ nanocomposites. *Prog. Org. Coat.* **2017**, *112*, 176–186. [[CrossRef](#)]

35. Nonahal, M.; Rastin, H.; Saeb, M.R.; Sari, M.G.; Moghadam, M.H.; Zarrintaj, P.; Ramezanzadeh, B. Epoxy/PAMAM dendrimer-modified graphene oxide nanocomposite coatings: Nonisothermal cure kinetics study. *Prog. Org. Coat.* **2018**, *114*, 233–243. [[CrossRef](#)]
36. Friedman, H.L. Kinetics of thermal degradation of char-forming plastics from thermogravimetry. Application to a phenolic plastic. *J. Polym. Sci. Part C Polym. Symp.* **1964**, *6*, 183–195. [[CrossRef](#)]
37. Vyazovkin, S.; Burnham, A.K.; Criado, J.M.; Pérez-Maqueda, L.A.; Popescu, C.; Sbirrazzuoli, N. ICTAC Kinetics Committee recommendations for performing kinetic computations on thermal analysis data. *Thermochim. Acta* **2011**, *520*, 1–19. [[CrossRef](#)]
38. Venkatesh, M.; Ravi, P.; Tewari, S.P. Isoconversional kinetic analysis of decomposition of nitroimidazoles: Friedman method vs Flynn-Wall-Ozawa method. *J. Phys. Chem. A* **2013**, *117*, 10162–10169. [[CrossRef](#)]
39. Kissinger, H.E. Reaction kinetics in differential thermal analysis. *Anal. Chem.* **1957**, *29*, 1702–1706. [[CrossRef](#)]
40. Ebrahimi-Kahrizangi, R.; Abbasi, M. Evaluation of reliability of Coats-Redfern method for kinetic analysis of non-isothermal TGA. *Trans. Nonferrous Met. Soc. China* **2008**, *18*, 217–221. [[CrossRef](#)]
41. Turmanova, S.C.; Genieva, S.; Dimitrova, A.; Vlaev, L. Non-isothermal degradation kinetics of filled with rice husk ash polypropylene composites. *Express Polym. Lett.* **2008**, *2*, 133–146. [[CrossRef](#)]
42. Huang, C.C.; Wu, T.S.; Leu, A.L. Determination of kinetic parameters for decomposition reaction from a single DTA curve. *Thermochim. Acta* **1991**, *188*, 119–128. [[CrossRef](#)]
43. Šesták, J.; Berggren, G. Study of the kinetics of the mechanism of solid-state reactions at increasing temperatures. *Thermochim. Acta* **1971**, *3*, 1–12. [[CrossRef](#)]
44. Liu, X.; Hao, J.; Gaan, S. Recent studies on the decomposition and strategies of smoke and toxicity suppression for polyurethane based materials. *RSC Adv.* **2016**, *6*, 74742–74756. [[CrossRef](#)]
45. Gallo, E.; Scharrel, B.; Acierno, D.; Russo, P. Flame retardant biocomposites: Synergism between phosphinate and nanometric metal oxides. *Eur. Polym. J.* **2011**, *47*, 1390–1401. [[CrossRef](#)]
46. Van Krevelen, D.W.; Te Nijenhuis, K. *Properties of Polymers: Their Correlation with Chemical Structure; Their Numerical Estimation and Prediction from Additive Group Contributions*; Elsevier: Amsterdam, The Netherlands, 2009.
47. Vimalathithan, P.K.; Barile, C.; Casavola, C.; Arunachalam, S.; Battisti, M.G.; Friesenbichler, W.; Vijayakumar, C.T. Thermal degradation kinetics of polypropylene/clay nanocomposites prepared by injection molding compounder. *Polym. Compos.* **2019**, *40*, 3634–3643. [[CrossRef](#)]

